PROCEEDINGS, Thirty-Fifth Workshop on Geothermal Reservoir Engineering
Stanford University, Stanford, California, February 1-3, 2010
SGP-TR-188

TRACER TESTS IN THE ENHANCED GEOTHERMAL SYSTEM (EGS) OF SOULTZ–SOUS–FORÊTS. WHAT DOES THE STRATIFIED MEDIUM APPROACH TELL US ABOUT THE FRACTURE PERMEABILITY IN THE RESERVOIR?

Giovanni Radilla[1], Judith Sausse[2], Bernard Sanjuan[3], and Mostafa Fourar[1]

[1]LEMTA, Nancy-University, CNRS,
2 Avenue de la Forêt de Haye, BP 160,
54504 Vandoeuvre Cédex, France
e-mail: Giovanni.Radilla@ensem.inpl-nancy.fr

[2]G2R, Nancy-University, CNRS, CREGU
BP 70239,
54506 Vandoeuvre Cédex, France

[3]BRGM,
3 Avenue Claude Guillemin,
45065 Orléans Cédex 02, France

ABSTRACT

We present a new interpretation of tracer tests performed in 2005 in the French EGS located at Soultz-sous-Forêts. A previous analysis of fluorescein tests (Sanjuan et al., 2006) revealed substantial differences in terms of connectivity between the injection well (GPK3) and the two production wells (GPK2 and GPK4). The tracer concentration in the fluid discharged from the production wells was measured and partially modeled using a code based on a model of dispersive transfer. The results suggested the existence of at least three fluid circulation loops. Two of them (loops 1 and 2) associated to GPK2, and the third one (loop 3) associated to GPK4.

Our new analysis is based on the equivalent stratified porous medium model. In this approach, each circulation loop, which corresponds to a flow path through the rock formation, is regarded as a stratified porous medium having a log-normal permeability distribution. The heterogeneity of this equivalent porous medium is quantified by the stratification factor defined as the standard deviation to the mean permeability ratio.

The results of this work allowed a very accurate modeling of the concentration curves for both production wells. The stratification factors show that the three circulation loops have different levels of heterogeneity. In addition, the tracer mean arrival times are in a ratio of 4.3 between loop 2 and loop 1, and 13.6 between loop 3 and 1 thus giving some insight on the mean permeabilities of the equivalent stratified media.

This tracer test model is compared to a new deterministic 3D model of the fracture zones observed in the Soultz granitic reservoir. The major fracture zones encountered around 6 wells (4550, EPS1, GPK1, GPK2, GPK3 and GPK4) are located and characterized in terms of size, orientation, extensions and widths: fracture zones, microseismic structures and structures derived from vertical seismic profiles are modeled using Discrete Fracture Network tools of the gOcad modeling platform (Paradigm, Earth Decision Sciences). The objective is to match the permeability results derived from the tracer test modeling and from the geometry of the Soultz fracture network to try to better understand the geothermal fluid flow pathways in the reservoir.

INTRODUCTION

Soultz-sous-Forêts, located in the Upper Rhine Graben, hosts one of the few deep geothermal 'Enhanced Geothermal System' test sites in the world. At its current state of development, the EGS site consists of three boreholes: GPK2, GPK3 and GPK4, the European geothermal pilot plant which extends to more than 5000 m depth, GPK1 a first hydraulic test well which extends to 3600 m and a reference hole EPS1 which has been fully cored down to 2230 m.

In deep enhanced geothermal systems (EGS), natural or forced fluid circulation takes place through the fracture networks in crystalline rocks characterized by low matrix porosity. The connection between fractures and the consequent anisotropic permeability are then crucial to insure the efficiency of the geothermal exchanger and to recover sufficient fluid temperatures at surface.

The objective of this paper is therefore an attempt to match and model the 2005 tracer test interpretation

results proposed by Sanjuan et al. 2006 with the knowledge we have of the 3D network of connected, permeable fractures within the target rock volume between the wells (Sausse et al., 2010).

The final objective of this study is to achieve a better understanding and prediction of the hydraulic response of the granite respecting the structural observations of fault and fracture organizations.

TRACER TEST

A tracer test using 150 kg of 82.5% pure fluorescein and a chemical fluid monitoring program accompanied the 5-month circulation experiment carried out between injection well GPK3 and production wells GPK2 and GPK4 in July–December 2005 (Sanjuan et al., 2006). Preliminary operations, including 4 days of production from GPK2 and GPK4, were performed before initiating the circulation test. During the test, the geothermal fluid discharged from wells GPK2 and GPK4 was injected into GPK-3. At the end of the experiment, some fresh water was also injected into GPK-3.

The injection rate was estimated to be close to 15 l/s, with 11.9 l/s coming from GPK2 and 3.1 l/s from GPK4. Based on these values, about 209,000m^3 of fluid were injected into GPK3, and 165,500m^3 and 40,500m^3, respectively, were discharged from GPK2 and GPK4. Geochemical sampling and analyses were performed on the discharged and injected fluids, including fluorescein analysis, on-site conductivity, pH, Eh, dissolved oxygen, alkalinity, and Cl, SO4, Na, K, Ca, Mg, SiO2, Br, Li concentrations. Some of the fluid samples were analyzed for naphthalene sulfonate tracers at the BRGM laboratories. Detailed tables of analytical data are reported in Sanjuan et al. (2006). These authors demonstrate that 2 types of circulation are developed between the wells. These tests gave evidence of a fast and relatively direct hydraulic connection between GPK3 and GPK2 (short loop) but also indicated the existence of another larger and slower hydraulic connection between GPK3 and GPK4 (large loop).

3D MAIN FAULT NETWORK

An important database of geological data (Genter et al., 1995), well logs (Dezayes et al., 1995; 2005; 2010; Sausse and Genter, 2005; Sausse et al; 2006), microseismicity recordings (Cuenot et al., 2007; 2008; Dorbath et al., 2009) and Vertical Seismic Profiling (VSP) results are compiled and combined to build a new original 3D model of the Soultz-Sous-Forêts fractured reservoir (Sausse et al., 2010).

The main well logging in the three deepest wells (GPK2, GPK3 and GPK4) consisted of the gamma-ray spectral log. Fracture geometrical properties and their spatial relationships are analyzed based on amplitude and transit time anomalies derived from acoustic image logs (Ultrasonic Borehole Imager; UBI). The fractures can be identified with high accuracy and measured in azimuth and dip by this borehole imagery technique. Other flow and/or temperature logs were run in the different deep wells during injection and production tests and some interpretation of the main fracture and permeable zones is proposed by Dezayes et al. (2005 and 2010). These hydraulically active fractures could correspond to either isolated fractures or series of thin parallel fractures or large-scale fracture zones. These large-scale fracture zones reach 10 m in thickness and are characterized by sealed core and a peripheral damage zone that is highly fractured and therefore highly permeable (Genter et al., 2000). Fracture orientations and relative contribution to flow are available in the open holes for the three deepest wells (Sausse et al., 2007, 2008).

This fracture network, identified at the well scale, has been completed by other geophysical data at the reservoir scale.

Numerous hydraulic stimulations performed have been performed at Soultz between 2000 and 2005 and have generated micro-seismic activity that has been interpreted in terms of major structures (Sausse et al., 2010). Events locations from Dorbath et al. (2009) were put into relation with the fault organization.

Then some VSP data (1993 survey) have been re-interpreted in GPK1 and EPS1 after a specific processing (Place et al., 2007). Thanks to a high signal/noise ratio of these records, polarization analysis has been carried out: the arrivals show much more energy on the vertical component than on the horizontal components, suggesting a vertical polarization. At the well location, these seismic events are recognized at depth levels where the GPK1 well intersects highly permeable faults (Evans et al., 2005).

Based on these seismic and structural data, a complete 3D model of the Soultz-Sous-Forêts reservoir fracture network matched in details with the granite lithology, geophysical and hydraulic characteristics is now available (Sausse et al. 2010). Finally, 53 structures are defined in the vicinity of the geothermal plant and between depths of 800 to 6000 m TVDSS. 39 fracture zones, 7 microseismic structures and 6 VSP derived structures are represented in the 3D model (Figure 1 and Table 1). The matching of these various geophysical approaches shows that fractures described at the well scale could be extrapolated at the reservoir scale to propose new guides for a global 3D model of the Soultz geothermal reservoir.

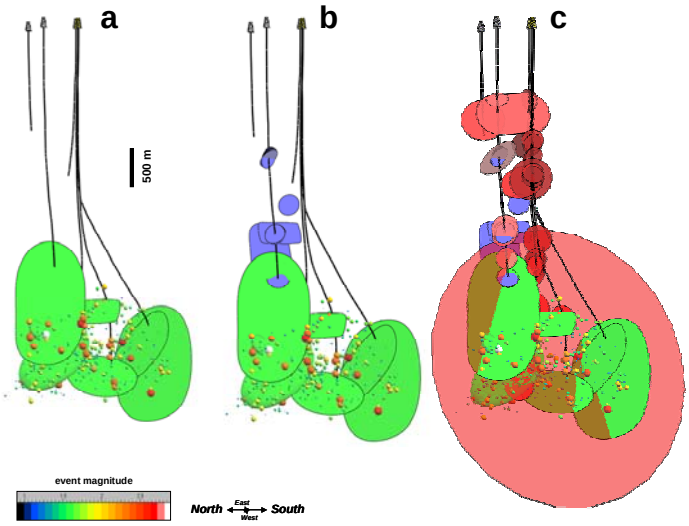

Figure 1: North-South vertical view of the final 3D model structures defined from well logging analysis (red discs), from the interpretation of the microseismicity following the hydraulic stimulations of the three deepest wells GPK2, GPK3 and GPK4 (green discs) and the VSP EPS1 and GPK1 interpretations (blue discs)

Well	Name	Depth (MD)	2*dh	2*dv	Dip direction °	Dip °	fit with
EPS1	EPS1-FZ1010	1012	300	300	130	79	
	EPS1-FZ1200	1198	600	600	247	74	
	EPS1-FZ1640	1643	400	400	76	58	
	EPS1-FZ2180	2179	600	600	278	53	
	VSP-EPS1-NI	not observed at the well scale	300	300	65	70	/
GPK1	GPK1-FZ1015	1015	300	300	270	45	
	GPK1-FZ1220	1220	600	600	247	74	
	GPK1-FZ1820	1820	600	600	27	47	
	GPK1-FZ2815	2815	400	400	230	70	
	GPK1-FZ3220	3223	300	300	60	75	
	GPK1-FZ3490	3492	300	300	257	63	GPK3*-FZ4770
	GPK1-FZ2870	2868	300	300	290	70	
	VSP-GPK1-1800		300	300	same than GPK1-FZ1820		GPK1-FZ1820
	VSP-GPK1-2860		300	300	same than GPK1-FZ2870		GPK1-FZ2870
	VSP-GPK1-3490		300	600	257	55-65	GPK3-FZ4770* and GPK1-FZ3490
	VSP-GPK1-NI1	not observed at the well scale	600	300	250	85	/
	VSP-GPK1-NI2	not observed at the well scale	600	1000	250	55	/
	MS-GPK3-2003a	3492	1000	2000	257	63	GPK1-FZ3490
	GPK3-FZ4770*	4775	3000	3000	234	**71**	
GPK2	GPK2-FZ2120	2123	600	600	65	70	
	GPK2-FZ3240	3242	300	300	82	69	
	GPK2-FZ3350	3347	300	300	231	84	
	GPK2-FZ3515	3514	300	300	313	57	
	GPK2-FZ3900	3900	400	400	234	64	
	GPK2-FZ4760	4760	400	400	250	65	
	GPK2-FZ4890	4890	300	300	250	65	
	GPK2-FZ5060	5060	400	400	250	65	
	MS-GPK2-2000a	not observed at the well scale	600	1200	244	86	GPK3-FZ4770
	MS-GPK2-2000b	not observed at the well scale	200	300	not defined		GPK3-FZ4770 and GPK1-FZ3490
GPK3	GPK3-FZ1580	1579	300	300	69	78	
	GPK3-FZ1640	1637	300	300	46	68	
	GPK3-FZ1820	1820	300	300	46	64	
	GPK3-FZ2040	2042	300	300	72	65	
	GPK3-FZ2045	2046	300	300	243	69	
	GPK3-FZ2090	2092	300	300	91	76	
	GPK3-FZ2970	2970	400	400	77	82	
	GPK3-FZ3270	3271	400	400	345	85	
	GPK3-FZ4090	4089	300	300	253	62	
	GPK3-FZ4770	4775	3000	3000	234	64	original orientation
	GPK3-FZ4770*	4775			234	**71**	final orientation
	MS-GPK3-2003a	not observed at the well scale	1000	2000	257	63	GPK1-FZ3490
	MS-GPK3-2003b	not observed at the well scale	600	400	270	45	/
	MS-GPK3-2003c	not observed at the well scale	1000	600	261	67	/
GPK4	GPK4-FZ1720	1723	300	300	216	69	
	GPK4-FZ1800	1801	300	300	26	80	
	GPK4-FZ2820	2817	300	300	242	86	
	GPK4-FZ3940	3940	300	300	250	68	
	GPK4-FZ4360	4361	400	400	280	77	
	GPK4-FZ4620	4620	300	300	285	78	
	GPK4-FZ4710	4712	400	400	212	50	
	GPK4-FZ4970	4973	300	300	276	81	
	GPK4-FZ5010	5012	300	300	257	85	
	GPK4-FZ5100	5100	300	300	255	69	
	MS-GPK4-20045a	4620	600	1200	same than GPK4-FZ4620		GPK4-FZ4620
	MS-GPK3-20045b	4973	1000	1500	same than GPK4-FZ4973		GPK4-FZ4970
	GPK3-FZ4770*	4775	3000	3000	234	**71**	
4550	4550-FZ1265	1265	600	600	260	75	

Table 1: Final structural and geometrical data of the 3D model structures defined from well logging analysis, from the interpretation of the microseismicity following the hydraulic stimulations of the three deepest wells GPK2, GPK3 and GPK4 and the VSP EPS1 and GPK1 interpretations. Geometrical parameters characterizing the main fracture zones with measured depths, extensions of major axis dv and minor axis dh, dip direction and dip. Each well is characterized by several fracture zones identified by a nomenclature name: well name-FZ-Measured Depth of the fracture centre. Correlation and matching between VSP, microseismic and structural data are mentioned (Sausse et al. 2010).

WELL SCALE FRACTURES

Centimetric fractures could be detected thanks to the accurate U.B.I. vertical resolution of 0.5 to 1 cm. This database has been therefore completed with a new study that focuses only on open fractures that host fluid flows in the reservoir (Massart et al. 2010). However, the real effective opening of a fracture remains difficult to define. Closed fractures are sealed by secondary re-crystallization or filled with fine impermeable particles (only amplitude traces on U.B.I.). The main faults present damage zone and largely open fractures (both amplitude and transit time traces on U.B.I.). Between these two extreme opening states, several other types of fracture width are proposed in this study.

A total of 1878 open fractures were located on GPK2, GPK3 and GPK4 UBI logs, amongst which 1637 were defined as natural open fractures (labels 1 to 6) , 82 were defined as damage zones (label 7) and 159 were defined as horizontal induced drilling fractures (label 8). For each fracture, its measured depth, true dip, dip direction, and aperture (continuous or fragmented sinusoids) are recorded.

Previous other main fracture zones (Sausse et al., 2010; Dezayes et al., 2010) are characterized by labels 11 to 14.

Fracture widths

This new high resolution fracture database includes all fracture types, faults and damage zones observed in the wells GPK2, GPK3 and GPK4 (Figure 2) and are analyzed using the relation between fracture occurrences (probability of fracture intersection with the wells) and widths such as proposed by Bonnet et al. (2001). The damage zones do not represent strictly fractures, but their vertical extension along the wells was assimilated to the width of the associated faults previously defined by Dezayes et al. (2010) and Sausse et al. (2010). For example, the major fault that intercepts the well GPK3 at 4775 m (M.D.) is surrounded by a damage zone of 13 m. This fault is therefore characterized by a 13 m width equal to its damage zone width in the database. In Figure 2 is presented a bi-logarithm diagram that plots the number of fractures *n* of each label as a function of their mean width *W*. White dots in Figure 2 correspond to the fracture labels that are correlated over a large magnitude of fracture widths. In black are plot "problematic" points, corresponding to fracture labels 5 and 6. This relation is well fit to a power law equation with an exponent equal to 1.04.

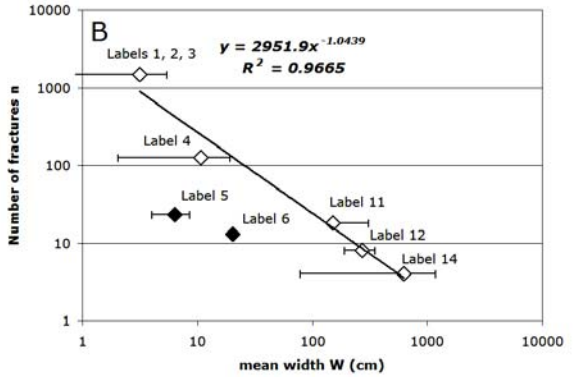

Figure 2: Bi-logarithm diagram representing the number of fractures n as a function of their width W in cm. Labels 5 and 6 that are not correlated to the general trend are removed of the database for the calculation of the cumulative probability. Labels 11, 12 and 14 correspond to faults which damage zones were located on U.B.I. images. Label 11 corresponds to the littlest faults and Label 12 to the medium one in term of fracture sizes. Label 14 corresponds to the main fault of the Soultz reservoir.

The general trend observed on Figure 2 is not adapted to describe fracture labels 5 and 6 that represent continuous or wide open fractures on U.B.I. images. These fractures are not sufficiently numerous to fit with the general trend. One possible explanation could be that in this study only open fractures were taken into account. Indeed, a lot of same types of fractures are today totally sealed by sequences of hydrothermal alteration. These sealed fractures were generated in the same time than those described by labels 5 and 6 and today still open. The paleo-fractures present similar widths than the still open ones but sealed widths. These wide open and continuous open fractures are the main fractures that could be percolated within the rock mass insuring the pervasive alteration of the granite when big faults generate more localized vein alteration (Sausse and Genter, 2005). A first explanation of this underestimation of the number of fracture labels 5 and 6 could therefore be that the missing fractures labels 5 and 6 are now sealed and therefore not take into account in the database.

Fracture labels 1, 2 and 3 are merged in one single group in the plot of Figure 2 because of the huge proportion of labels 1 in the database that mask the influence of 50% and 75% continuous fracture traces. This distinction is therefore not discriminatory in this study.

A low fractal dimension such as 1.04 indicates that fractures are strongly clustered. This organization of very dense zones of fractures around the main fault corridors is well known at Soultz (Sausse and Genter, 2005).

Fracture lengths

Johnston (1996) proposes a relation between width and extension. Collecting data for five study areas with widely varying structural geometries in a variety of host rock types, they determine that the extension and the width of a fracture are proportional in some cases but that they follow a more generalized power-law of the form:

$$L = k W^{d} \quad (1)$$

where k is a coefficient characteristic of the facies ranging from 20 to 2000 for granitic facies, and d the fractal dimension of the fracture set. The coefficient k is higher in extensional context than in compression one, ranging from 57 to 1231 with a mean value of 402.

We decided then to follow the hypothesis of Johnston (1996) and we chose to calculate the mean extension of the different labels using values of $k = 400$ and $d = 1.04$. The results are reported in Table 2.

	Label & fracture type	Mean widths W (cm)	Mean extensions L (m)
1	Discontinuous open traces (25%)	3.15	11
2	Discontinuous open traces (50%)		
3	Discontinuous open traces (75%)		
4	Vuggy Fractures	10.69	39
5	Continous open fractures	6.32	23
6	Wide open fractures	20.31	76
11	minor faults	150.11	610
12	medium faults	269.83	1123
14	major faults	626.53	2697

Table 2: Mean fracture extensions and widths by fracture labels.

The width of the damage zone associated to the major fault at Soultz is equal to 13 m. By application of the previous formula, its extension is therefore equal to 2.7 km which could be a correct estimation because this fault crosses the three wells on a minimum distance of 2 km.

Fracture conductivity at well scale

Fracture equivalent conductivity (κ) was estimated using the model proposed by Snow, 1969; Oda, 1986; Ababou, 1991 and Sausse et al., 1998. This approach proposes to quantify equivalent hydraulic properties on the basis of the geometric parameters of fractures (mainly apertures and spacing). Two assumptions are done with 1) a Poiseuille law to model the flow in each individual fracture assumed to be an infinite plane at the scale of the well and 2) the assumption of a global and homogeneous pressure gradient in the reservoir.

The following equation is proposed:

$$\kappa_i = \frac{g}{12\,\eta}\,\frac{A_i^3}{S_i} \quad (2)$$

Where g is acceleration due to gravity [9.81 m s^{-2}]; η, the kinematic viscosity of the fluid [water: 10^{-6} m^2 s^{-1}], A_i, the width of fracture i [m] and S_i, the mean spacing between fracture i and fractures i-1 and i+1 [m].

Vertical spacing are calculated between the fracture plane points along the wells. Each fracture plane is characterized by a constant aperture related to its label such as mentioned in Table 2.

These values are directly related to the value of the fracture widths quantified as damage zone around fractures on the UBI images. The computed conductivities stay therefore relative values in the objective of a comparison of the well hydraulic behaviors. They are therefore not physically significant in terms of quantitative and realistic flows.

Results show that some clear differences appear between the wells. For example the mean fracture conductivities ± standard deviations are equal to 5.38 10^3 ± 2.44 10^4 and 1.55 10^1 ± 7.07 10^4 m/s respectively for GPK2 and GPK4, the production wells and 6.22 10^5 ± 1.79 10^7 m/s for GPK3, the injection well during the tracer test.

However, the standard deviations are quite large indicating that fractures are clustered in the wells and display quite various damage zone widths especially for the main fault zones.

Figure 3 presents the distribution of fracture conductivities using a logarithm X scale and show this great dispersion of the values and a highest proportion of thin fractures (κ_i between 1 and 10 m/s) for GPK2.

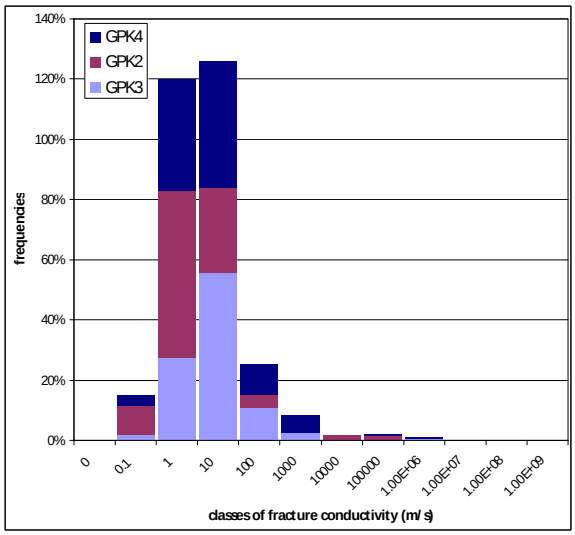

Figure 3: Distribution of the fracture relative conductivities for the three deep wells.

This clustering is also illustrated by the variation coefficient *Cv* i.e. the ratio between the standard deviation and the mean values of the conductivities of fractures along the three well paths. *Cv* values are equal respectively to 29, 5 and 4564 for GPK3, GPK2 and GPK4. The highest dispersion of conductivity value is observed for GPK4 indicating very different values of conductivities and mainly spacing with therefore the possibility of shortcuts by big faults in this zone of the reservoir. On the contrary, values are more homogeneously distributed around GPK2 indicating a better distributed fracture network along the well path and possibly a more homogeneous equivalent porous media constituted by thinner but better connected fractures.

MODELING OF THE TRACER TEST RESTITUTION CURVES

Figures 4 and 5 show respectively the dimensionless fluorescein concentration measured on GPK2 and GPK4 during the tracer circulation test.

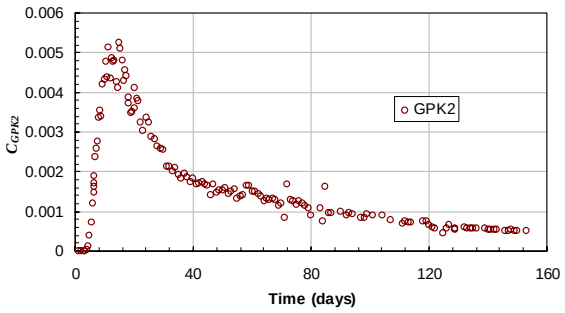

Figure 4: Dimensionless concentration (GPK2)

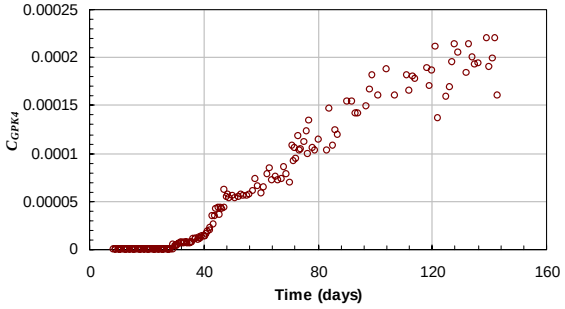

Figure 5: Dimensionless concentration (GPK4)

As suggested by Sanjuan et al., 2006 the long tracer concentration trail observed in GPK2 is attributed to a high heterogeneity in the rock formation between GPK3 and GPK2.

One simple yet elegant way to model such dispersion behavior is the equivalent stratified medium approach in which a given heterogeneous porous medium is replaced by a stratified medium following a probability distribution in terms of permeability. In this approach, dispersion is the result of permeability heterogeneity alone which is characterized by the stratification factor, *H*:

$$H = \sigma_K / \overline{K} \tag{3}$$

σ_K and $\overline{K}$ are the standard deviation and the mean value of the permeability distribution. The most commonly used permeability distribution for real heterogeneous media is the lognormal distribution. In that particular case and for a concentration step, the dimensionless concentration *C* at distance *x* from the injection section and at time *t* is given by (Fourar, 2006; Fourar and Radilla, 2009):

$$C = \frac{1}{2}\operatorname{erfc}\left(\ln\left(\frac{x}{Ut}\sqrt{1+H^2}\right)\Big/\sqrt{2\ln\left(1+H^2\right)}\right) \tag{4}$$

where $U = Q/(A\phi)$ is the mean velocity of the tracer front in the equivalent porous medium, *Q* is the volumetric flow rate, *A* is the cross section area, and ϕ is the porosity.

As the tracer was injected during one day, we used Eq. (4) to produce both the response to a positive concentration step injected at $t = 0$ days, and to a negative concentration step injected at $t = 1$ day. The sum of the two responses gives us the concentration corresponding to the real tracer injection. This approach has also the advantage to allow injecting easily the right amount of tracer mass.

This procedure was applied separately for each one of the circulation loops and leaded to the corresponding concentration curves ($C_1(t)$, $C_2(t)$ et $C_3(t)$).

Because the production wells discharge not only fluid coming from the injection well through the circulation loops but also fluid coming from the rock formation itself at zero tracer concentration, the relationships between the measured concentrations C_{GPK2} and C_{GPK4}, the calculated ones ($C_1(t)$, $C_2(t)$ and $C_3(t)$), and the corresponding volumetric flow rates Q_i are:

$$C_{GPK2}(Q_1 + Q_2 + Q_{e2}) = C_1(t)Q_1 + C_2(t)Q_2 + 0\,Q_{e2} \tag{5}$$

$$C_{GPK4}(Q_3 + Q_{e4}) = C_3(t)Q_3 + 0\,Q_{e4} \tag{6}$$

and rearranging, we obtain

$$C_{GPK2} = \frac{Q_1}{Q_{T2}}C_1(t) + \frac{Q_2}{Q_{T2}}C_2(t) \tag{7}$$

$$C_{GPK4} = \frac{Q_3}{Q_{T4}}C_3(t) \tag{8}$$

In order to model the concentration curves of Figures 4 and 5, we used equations (4), (7) and (8) for each circulation loop. The fitted parameters for loop *i* are:

- the mean arrival time, x/U_i
- the stratification factor, H_i
- the dilution ratio (Q_i/Q_T)

The sensitivity of the calculated concentrations to the parameters of the model was analyzed. Results showed that sensitivities of the different parameters are not correlated to each other and therefore allowing us to fit all the parameters independently from one another.

The results of the modeling are presented in Table 3 and Figures 6 and 7 show that the estimated parameters allow a very accurate modeling of the measured tracer concentration in both production wells.

Production well	GPK2		GPK4
Circulation loop	1	2	3
Mean arrival time, x/U (days)	13.9	60.2	188.2
Stratification factor, $H = \sigma_K / \overline{K}$	0.556	0.943	0.718
Dilution ratio	0.0797	0.1774	0.0604

Table 3: Results of the modeling of the concentration curves using the equivalent stratified model approach on the three circulation loops.

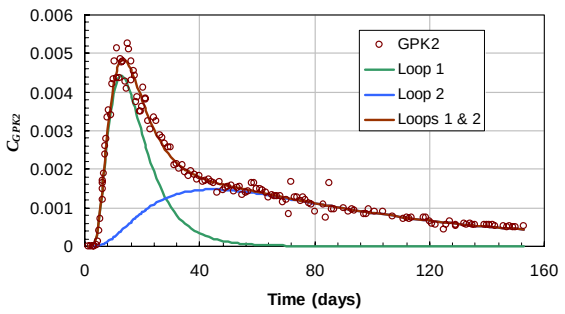

Figure 6: Dimensionless concentration (GPK2)

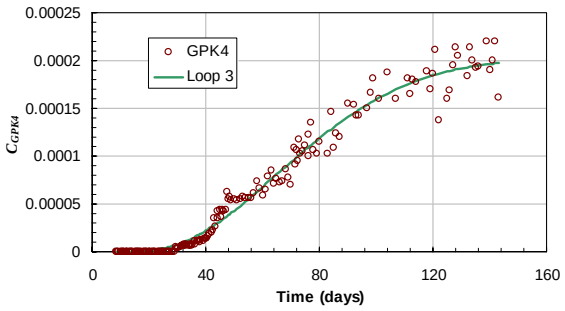

Figure 7: Dimensionless concentration (GPK4)

Table 3 shows mean arrival times spreading from 13.9 days to 188.2 days, thus confirming the already observed important differences in connectivity between the three loops (Sanjuan et al., 2006). Values of the stratification factors show that loop 2 is the most heterogeneous while loop 1 is the less heterogeneous. Finally, dilution ratios clearly show that the geothermal fluid is dominant in the discharged fluids from both production wells.

Values presented in Table 3 allow further analysis of the circulation loops.

During the tracer circulation tests, the flow rates injected into GPK3 and discharged from GPK2 and GPK4 were measured and the corresponding values are 15 l/s, 11.9 l/s, and 3.1 l/s. Therefore, the dilution ratios in Table 3 allow us to calculate the flow rates Q_i circulating in each loop and also the *external* flow rates (i.e., which don't come from the injection well) Q_{e2} and Q_{e4}.

The distance between the injection well and the two production wells is about the same (around 600 m). If we assume that the equivalent porous media linked to the three circulation loops are also 600 m long, we can calculate the mean velocities U_i. As we already mentioned the mean velocities are given by $U = Q/(A\phi)$ and therefore, we are able to calculate the effective cross section area, $A\phi$ for each loop. As the length of the loops is known (600 m), the total volume of fluid within the loop can be calculated.

Table 4 summarizes those results:

Production well	GPK2		GPK4
Circulation loop	1	2	3
Total discharged flow rate (l/s)	11.9		3.1
External flow rate, Q_e (%)	74.3%		94%
External flow rate, Q_e (l/s)	8.84		2.91
Volumetric flow rate (l/s)	0.95	2.11	0.19
Mean velocity, U (m/day)	43.26	9.96	3.19
Effective cross section area, $A\phi$ (m^2)	1.9	18.3	5.1
Fluid volume within the loop (m^3)	1137	10983	3043

Table 4: Further analysis of the circulation loops.

Each circulation loop is regarded as an equivalent porous media of mean permeability $\overline{K}$. Therefore, Darcy's law can be written for the *i*-th loop:

$$\left(\frac{\Delta P}{L}\right)_i = \frac{\mu}{\overline{K}_i} U_i \phi_i \qquad (9)$$

Loops 1 and 2 are connected to the same wells (GPK3 and GPK2). Thus, their equivalent stratified media are likely to share the same pressure gradient. Under this assumption the following relationship arises:

$$\frac{\mu}{\overline{K}_1} U_1 \phi_1 = \frac{\mu}{\overline{K}_2} U_2 \phi_2 \qquad (10)$$

Rearranging, we get:

$$\frac{\overline{K}_1\phi_2}{\overline{K}_2\phi_1} = \frac{U_1}{U_2} = 4.34 \quad (11)$$

It is important to emphasize that in the absence of data on the porosity of the fracture network between GPK3 and GPK2, it is not possible to calculate the ratio of mean permeabilities in loops 1 and 2.

However, under the assumption that $\phi_1 \approx \phi_2$, the average permeability of loop 1 would be 4.3 times that of loop 2:

$$\overline{K}_1 = 4.34\overline{K}_2 \quad (12)$$

Combining this last result to the stratification factors H_1 and H_2 of Table 3,we get:

$$\sigma_{K_1} = 2.56\sigma_{K_2} \quad (13)$$

In addition, linking the mean permeability of loop 3 to that of loops 1 or 2 requires the knowledge of the two pressure gradients: (GPK3-GPK2) and (GPK3-GPK4).

CONCLUSIONS

The Soultz reservoir is a fractured reservoir characterized by various classes of fracture type (Tables 1 and 2). These fractures are clustered along the well paths defining damaged zones around them and therefore high or low equivalent porous media. A first comparison of the well fracture conductivities was therefore tested to try to identify same types of media heterogeneity than those describe by the tracer test interpretation. Transit times between GPK2 and GPK3 are described by two main loops of 13.9 or 60.2 days for fluorescein recovery. This transit time is much longer to connect GPK3 and GPK4 with 188.2 days for fluorescein recovery, third loop.

The ratios of these transit times for the three main loops correspond in a first approximation to the heterogeneity of the equivalent media permeability hosting the fluids circulations. This heterogeneity could be directly linked to the fracture distributions as shown in the last section of the paper by means of equations (9) to (13).

For example the ratio between the mean conductivities of GPK3 (6.22 10^5 m/s) and GPK2 (5.38 10^3 m/s) is equal to 116. The same ratio between GPK3 (6.22 10^5 m/s) and GPK4 (1.55 10^5 m/s) is strongly highest and equal to 40185.

These differences of fracture conductivities, main drains in the granite impermeable matrix, could explain the quick transfer of fluid between GPK2 and GPK3. Fluids are flowing between wells with same ranges of permeability and in an equivalent porous media constituted by thinner but highly connected fractures homogeneously distributed in this zone of the reservoir. On the contrary, the differences of conductivity ranges between GPK3 (high conductivities) and GPK4 (low conductivities) could imply that this transfer of fluids is more complicated in a more heterogeneously distributed porous media where fault zones, isolated, could control the fluid flows. Such a fault is for instance represented by the huge structure GPK3-FZ4770 (Table 1) that links directly GPK3 and GPK2 but outer of the reservoir open hole section avoiding any shortcuts of fluids between this two wells (Figure 1). This same fault is identified below the bottom hole section of GPK4 and we could think that GPK3-FZ4770 could make a shortcut of fluids and bring them towards deeper zones of the batholith implying longer pathways and therefore transit times for fluorescein recovery in GPK4.

REFERENCES

Ababou, R. (1991), "Approaches to large scale unsaturated flow in heterogeneous stratified and fractured geologic media", Section 4.2: Hydraulic properties of saturated fractured media, Report, NUREG/CR-5743, U.S. Nuclear Regulatory Commission, Washington.

Bonnet E., Bour O., Odling N., Davy P., Main I., Cowie P. and Berkowitz B. (2001), "Scaling of fracture systems in geological media", *Geophysics*, **39**, 347-383.

Cuenot, N., Del Mar Mesa Salgado, M., Naville, Ch., Gérard, A. and Place, J. (2007), "Soultz VSP 2007 campaign in GPK3 and GPK4: operation report and preliminary results", in Proceedings of the EHDRA scientific conference 28-29 June 2007, Soultz-sous-Forêts, France.

Cuenot, N., Dorbath, C., Dorbath, L. (2008), "Analysis of the Microseismicity Induced by Fluid Injections at the EGS Site of Soultz-sous-Forêts (Alsace, France): Implications for the Characterization of the Geothermal Reservoir Properties", *Pure appl. geophys.* **165**, 797-828.

Dezayes, C., Chevremont, P., Tourlière, B., Homeier, G., and Genter, A. (2005), "Geological study of the GPK4 HFR borehole and correlation with the GPK3 borehole (Soultz-sous-Forêts, France)", Final Report, BRGM report, Orléans, France, RP-53697-FR.

Dezayes, C., Genter, A. and Valley, B. (2010), "Structure of the low permeable naturally fractured geothermal reservoir at Soultz", *Geosciences* (in press).

Dezayes, C., Villemin T., Genter, A., Traineau, H., and Angelier, J. (1995), "Analysis of Fractures in Boreholes of Hot Dry Rock Project at Soultz-

sous-Forêts (Rhine Graben, France)", *Journal of Scientific Drilling*, **5** (1), 31-41.

Dorbath, L., Cuenot, N., Genter, A. and Frogneux, M. (2009), "Seismic response of the fractured and faulted granite of Soultz-sous-Forêts (France) to 5 km deep massive water injections", *Geophysical International Journal*, 1-23.

Evans, K. F., Genter, A., and Sausse, J. (2005), "Permeability creation and damage due to massive fluid injections into granite at 3.5 Km at Soultz: Part 1 - borehole observations", *Journal of Geophysical Research*, **110** (B04203), 0-19.

Fourar, M. (2006). Characterization of heterogeneities at the core-scale using the equivalent stratified porous medium approach. SCA International Symposium. Trondheim, Norway.

Fourar, M. and Radilla, G. (2009), Non-Fickian description of tracer transport through heterogeneous porous media. *Transport in Porous Media* (80)3, p. 561-579.

Genter, A., Traineau, H., Dezayes, C., Elsass, P., Ledésert, B., Meunier A. and Villemin T. (1995), "Fracture analysis and reservoir characterization of the granitic basement in the HDR Soultz project (France)", *Geothermal Science & Technology*, **4** (3), 189-214.

Genter, A., Traineau, H., Ledésert, B., Bourgine, B., and Gentier, S. (2000), "Over 10 years of geological investigations within the HDR Soultz project, France", in Proceedings of the World Geothermal Congress 2000, Kyushu-Tohoku, Japan.

Johnston, J.-D. and Mc Cafrey, K. (1996), "Fractal geometries of vein systems and the variation of scaling relationships with mechanism". *Journal of Structural Geology*, **18**, 349-358

Massart B., Paillet M., Henrion V., Sausse J., Dezayes Ch., Genter A. (2010), "Fracture Characterization and Stochastic Modeling of the Granitic Basement in the HDR Soultz Project (France)", in Proceedings of the World Geothermal Congress 2010, Bali, Indonesia.

Oda, M. (1986), "An equivalent continuum model for coupled stress and fluid flow analysis in jointed rock masses", *Water Ressources Research*, **22**, 1845-1856.

Place, J., Cox, M. and Naville, C. (2007), "Oriented 3C VSP (three component Vertical Seismic Profiling) applied to the delineation of highly dipping faults in a deep granitic basement", in Proceedings of the EHDRA scientific conference 28-29 June 2007, Soultz-sous-Forêts, France.

Sanjuan, B., Pinault, J. L., Rose, P., Gerard, A., Brach, M., Braibant, G., Crouzet, C., Foucher, J. C., Gautier, A. and Touzele, S. (2006), "Tracer testing of the geothermal heat exchanger at Soultz-sous-Forêts (France) between 2000 and 2005", *Geothermics*, **35** (5-6), 622-653

Sausse, J., and Genter, A. (2005), "Types of fracture permeability in granite", *Special Publication of the Geological Society of London* (Harvey, P. K., Brewer, T. S., Pezard, P. A. & Petrov, V. A. (eds), **240**, 1-14.

Sausse, J., Dezayes Ch., Dorbath L., Genter A. and Place J. (2010), "3D model of fracture zones at Soultz based on geological data, image logs, induced microseismicity and vertical seismic profiles", *Geosciences* (in press)

Sausse, J., Dezayes, C. and Genter, A. (2007), "From geological interpretation and 3D modelling to the characterization of the deep seated EGS reservoir of Soultz (France)", in Proceedings European Geothermal Congress 2007, Unterhaching, Germany, 30 May-1 June 2007.

Sausse, J., Dezayes, C., and Genter, A. (2008), "Characterization of fracture connectivity and fluid flow pathways derived from geological interpretation and 3D modelling of the deep seated EGS reservoir of Soultz (France)", in Proceedings, 33rd Workshop on Geothermal Reservoir Engineering, Stanford University, Stanford, California, January 28-30.

Sausse, J., Fourar, M. and Genter, A. (2006), "Permeability and alteration within the Soultz granite inferred from geophysical and flow log analysis", *Geothermics*, **35** (5-6), 544-560

Sausse, J., Genter, A., Leroy, J.L., and Lespinasse, M. (1998), "Altération filonienne et pervasive: Quantification des perméabilités fissurales dans le granite de Soultz sous Forêts (Bas-Rhin, France)", *Bulletin de la Société Géologique de France*, **169** (5), 655-664.

Snow, D. T. (1969), "Anisotropic permeability of fractured media". *Water Resources Research*, **5**, 1273-1289.